Physical properties of Sn affected Cu through lead-free solder and combined effect of severe cold deformation and thermal ageing

M. S. Kaiser

Innovation Centre, International University of Business Agriculture and Technology, Dhaka-1230, Bangladesh

Abstract: The precipitation behavior of Cu, affected by lead free tin-based solder, is investigated as a function of cold deformation and artificial ageing using microhardness measurements, electrical resistivity, differential scanning calorimetry, reflectance behaviour and microstructural observation. The physio-electrical properties of pure Cu are greatly enhanced by changes in parameters like cold rolling and ageing when Sn is added through the solder. Cold rolling shows the superior hardness for Sn doped alloys because of the dissimilar crystal orientation of the BCC of Sn precipitated within the FCC Cu matrix. That is why it increases electrical resistivity. Two processes, namely precipitation strengthening through supersaturated solid solution and recovery, as well as recrystallization softening, are observed for the alloys. Fine precipitates, which hinder dislocation movement, improve recrystallization temperature, as confirmed by the DSC study. A spectral reflectance study reveals that Sn doping provides lower percent reflectance whereas it improves under ageing treatment due to the formation of fine precipitates. Micrograph studies confirm elongated grains in their rolling direction, and relatively thick grain boundaries as the presence of different particles for minor added alloys. Ageing at 400℃ for one hour all samples attain equiaxed grain by reaching a more or less recrystallized state.

*Corresponding author.
E-mail address:* dkaiser.res@iubat.edu (M. S. Kaiser).

1. Introduction

Among the main good-conducting materials in use, aluminum, copper, gold, and silver are the most well-known (Tehrani, 2020). Because of its unique qualities, copper is broadly used as a raw material in many industries and engineering sectors, including electronics, power generation, aerospace, and defense. Due to its superior electrical and thermal conductivity, as well as its reasonable cost in relation to gold and silver, it is primarily utilized for thermal management and electrical conduction services (Cañadilla et al., 2022; Davis, 1998; Kaiser & Kaiser, 2020). According to Sakib-Uz-Zaman and Khondokers (2023) review report, copper parts have superior antibacterial performance, better machinability, and high corrosion resistance, which makes them a good material for use in construction and automotive applications as well as medical devices. Many components, including heat exchangers, electronic connectors, springs, bearings, propulsion devices in aeronautical features, cooling channels, and gas turbines, are made with it. These days, the rapid expansion of industry necessitates more intricate geometries, structures, and ideal copper component qualities (Zhang et al., 2013).

Soldering copper is necessary in most cases in order for the operation to go smoothly (Narayan & Prabhu, 2013; Satyanarayan & Prabhu, 2012a). More precisely, it is used for joining or sealing copper pipes or heat exchanger tubes, connecting electrical wire, rewinding motors, jewellery, and other decorative items and other tasks related to the production and maintenance of printed circuit boards and other electronic components. The lead content of traditional soldiers is very high. Growing concerns about environmental and health effects have forced the removal of lead-based solders and the investigation of potential lead-free alternatives. On the other hand, lead toxicity has garnered a lot of attention due to the growing awareness of environmental protection. Laws banning the practice of lead in electronic packaging have been gradually implemented by the EU, Japan, and other nations and regions. These programs offer a promising platform for the creation of novel lead-free solders. Therefore, potential replacements for Sn-Pb solders include Sn-base lead-free solders, such as Sn-Ag, Sn-Bi, Sn-Cu, Sn-In, Sn-Sb, and Sn-Zn (Nai et al., 2015; Satyanarayan & Prabhu, 2011; Satyanarayan & Prabhu, 2013). The high tin content of the alternative potential materials presents unique difficulties for engineering applications. In most applications, the Sn-Ag-Cu solder, also referred to as SAC305 solder, at eutectic composition is now the industry standard. Lead-free Sn-Cu solder has garnered significant attention since it was first used in electronic packaging for its exceptional all-around performance and affordable price. Among the new alloy candidates free of lead, Sn-0.7Cu solders are cheap and show promise (Satyanarayan & Prabhu, 2012b; Zhao et al., 2019).

When the copper is recycled, it tends to accumulate some impurities from the melting environment, such as furnace refractory linings, reactors, launders, etc. Ahmed et al. (2021) also reported the addition of different elements due to repeated melting. This trend is even more pronounced when considering solder-affected Cu, which is heavily doped with tin and lead. The properties of aluminum can be modified by various processes, such as alloying, cold working, and thermal treatment (Rahman et al., 2021).

The physical behavior of copper in a broad sense microhardness, resistivity, reflectance, as well as microstructural properties—and the influence of the trace level of tin have been little studied by researchers in related fields such as the internet, libraries, and other information sources. Moreover, the implementation of plastic deformation along with thermal treatment is fully absent. Therefore, the present work is devoted to revealing the physico-electrical behavior of Sn-doped copper under work-hardening and heat treatment. To clarify the effects, two levels of the alloying elements, like Cu-0.26Sn and Cu-0.57Sn along with pure Cu is measured. Successful completion will result in the correct determination of the optimal structure, processing parameters, and properties of copper scrap, which is expected to find a wider application, especially in industries with better properties; some possible applications include films, plates, heat exchanger stacks, exhaust bellows, hydraulic and pneumatic equipment, etc. Local production of such components from materials obtained through recycling processes significantly reduces the burden of importing goods from abroad.

2. Materials and methods

Heat exchanger pipes contaminated by waste solder and leftover copper wires are collected from different sources. Some sections are cleaned by chopping off the soldered portion, while other sections are left the same and are simply cleaned with a wire brush to remove the solder. Kerosine oil is used to clean waste copper. Furthermore, using an appropriate flux cover, pure copper and both solder affected copper portions are melted in a pit furnace powered by natural gas. During melting, the temperature was maintained constantly at 1300±15°C, and before pouring, the melts were homogenizing with stirring and allowed to reach 1200°C. The casting was completed by pouring into an adjustable metal mould of mild steel, where the size was fixed at 20 x 150 x 300 mm. Before use, the inner surface of the mould was covered with clay film and preheated to 250°C. Using a Shimadzu PDA 700 optical emission spectrometer, the chemical compositions of three developed materials were examined.

The result showed that both solder affected cast samples contain not only two levels of small amounts of Sn but also trace impurities like pure Cu. The findings are shown in Table 1.

Table 1. Chemical composition of three samples by wt.%.

Alloy	Cu	Sn	Pb	P	Si	Zn	Al
Pure Cu	99.983	0.000	0.000	0.013	0.003	0.001	0.000
Cu-0.26Sn	99.502	0.257	0.006	0.130	0.102	0.002	0.001
Cu-0.57Sn	99.139	0.574	0.009	0.166	0.107	0.003	0.002

The sequence of heat treatment starts with homogenizing at 500°C for 12 hours, solution treatment at 750°C for a duration of 2 hours. Subsequently, the specimens are straight quenched into a salt ice water bath. The heat-treated samples were machined to 3.75 x 16 x 300 mm, 5 x 16 x 300 mm, 7.5 x 16 x 300 mm, and 15 x 16 x 300 mm sizes for the cold rolling operation. The cold rolling of 20, 40, 60, and 80% of solutionized alloys was done using a 10 HP capacity rolling mill, which gave a deformation of about 1.0 mm per pass and a final thickness of 3.0 mm each. Without rolling, specimens were recognized as 0% cold rolling. Cold rolled samples were subjected in to isochronal and isothermally ageing at different temperatures and times, respectively, using an Electric Muffle Furnace JSMF-30T ranging from 900± 3.0°C. A Mitutoyo HM-200 Series 810- Micro Vickers Hardness Testing Machine was used to measure the hardness of different alloys under various annealed conditions. With a 100gm load, both Vickers and Knoop indenters were used, and an indenter approach speed of 60 μm/s was used. The test force dwell time was considered to be twenty seconds. The sample size selected for this microhardness measurement was 3 x 15 x 15 mm. As a minimum, ten indentations were made at different places on each polished surface of the aged specimens prepared with fine-grade emery paper. A type 979 conductivity meter was used to measure the conductivity of alloys under various conditions. For these two measurements, 15 mm x 15 mm finished surfaces were created from the experimental three samples by grinding and polishing. Next, the conductivity data is converted to electrical resistance to display it graphically. A Shimadzu UV-2600 ISR Plus spectrometer was used to measure the ultraviolet-visible diffuse reflectance (UV-vis) spectra of powder made from the experimental alloys at room temperature in order to examine the reflectance response and its characteristics. Barium sulfate was employed as a 100% reflectance reference to ensure accurate baseline correction. Initially, the diffuse reflectance spectrum of BaSO$_4$ was recorded across the wavelength range of 220 nm to 800 nm. Following this, the synthesized alloy powder was consistently deposited into the BaSO$_4$ reference layer, and their diffuse reflectance spectra were recorded under alike measurement settings.

The solutionized and 80% deformed alloys were subjected to differential scanning calorimetry under a nitrogen gas atmosphere, where a heating run was used in a Du Pont 900 instrument. A lump of 65.0 mg each, was taken for the DSC scan, where a heating rate of 10°C/min was considered for temperatures ranging from 40°C to 550°C. Nagasaki-Maesono analysis as well as Kissinger plot was used to estimate the activation energy of transformations in the DSC heating run (Komesu et al., 2017). XRD analyses of the cold rolled and one-hour aged 100°C alloys were carried out using a PANalytical Empyrean X-ray diffractometer with Cu- Kα radiation and at a scanning rate of 1°/min and a Bragg angle 2θ ranging from 20° to 85°. The microstructures of the different possess samples were examined using Trinocular Inverted Metallurgical Microscope of model SKU: ME1200TB-10MA. Additionally, the surface morphology of the cold-worked and aged samples was examined using a JEOL JSM-7600F model field emission scanning electron microscope. The EDX spectra of the samples were recorded using a JEOL EX-37001 model electron dispersive spectrometer coupled with a FE-SEM setup. To observe the microstructure, copper etchant such as a 1:1 mixture of ammonium hydroxide and 3% hydrogen peroxide was used after the material had been polished with alumina.

3. Results and discussions

3.1. Microstructural study
3.1.1. Optical micrographs
The optical microstructures of commercially pure Cu and different Sn-added binary Cu-0.26Sn and Cu-0.57Sn alloys are shown in Fig 1. The samples are in a state of solution treatment and eighty percent cold-deformed, along with ageing at 400°C for one hour. Only after cold rolling and without ageing treatment is it observed that the crystal grains of the samples become blurry due to the strong cold deformation, making it impossible to discern between them (Fig. 1a-1c). The appearance of grains also elongated in the rolling direction due to plastic deformation. Copper's microstructure is made up mostly of α-Cu and a few minor impurities that are dispersed along the grain boundaries. The grain boundary, as a result, is thin. Primary copper, different Sn-based and trace intermetallics make up the Sn added alloys. Because of the different crystal structure of BCC β-tin and the higher atomic size of FCC Cu, it has a tendency to stay at the grain boundary, so the grain boundary is fairly thick. In the case of a higher added alloy, Sn makes it too thick.

Under higher ageing treatments, like 400°C for one hour alloy samples achieved the equiaxed grain structure through recrystallization. The microstructure of the samples under

such thermal treatment is demonstrated in Figure 1d-1f. The elongated grains are almost absent in the microstructure, and the grain boundaries are somewhat clear. All the added elements and trace intermetallic phases dissolve into the grain boundaries and Cu matrix. Again, the equiaxed grains, as related to pure Cu, are also thin, but Sn-added alloys consist of thick or thicker grain boundary depending on the amount of added elements. Contrarily, traces of indissoluble phases of Fe and Si may still be seen at the edges of grains as well as within them (Kaiser & Kaiser, 2021; Rahman et al., 2021).

3.1.2. SEM observation

For better clarification, the SEM images along with EDX spectra were further done on commercially pure Cu and the other two Sn affected alloys. Figure 2a- 2c consists of those as peak aged conditions, like aged at 200°C for one hour. Normally, at this ageing condition, the grain orientation of Cu and its alloys does not change. Just stress reliving accompanies with precipitation formation into the grain. But some differences

are observed between the three microstructures. As discussed in the optical microstructure section, for severe deformation, the crystal grains become distorted and elongate regularly in the rolling direction, making them difficult to distinguish. As usual, pure Cu displays the thin grain boundary, and the Sn-added alloy shows the thick grain boundary. Similarly, a higher addition of Sn makes it thicker (Peng et al., 2024; Yang et al., 2023). The corresponding EDX of the SEM of Cu reveals the following chemical composition by the weight percentage as 98.99% Cu, 0.32% Si, 0.23% Sn, 0.32%Pb and 0.14 % P. The EDX scan reveals the following chemical composition by weight percentage of Cu-0.26Sn Alloy as 96.98% Cu, 0.51% Si, 1.74% Sn, 0.55%Pb, 0.15%Fe and 0.07 % P. Similarly, Cu-0.57Sn alloy shows 94.03% Cu, 0.06% Si, 4.99% Sn, 0.52%Pb, 0.33%Fe and 0.07 % P. It is valid, but some variation is observed between the chemical analyzes presented in Table 1. It can be clarified that the specific selected area is very small and the samples have gone through various environments, such as ageing, polishing, etching, etc.

(a)   (b)   (c)

(d)   (e)   (f)
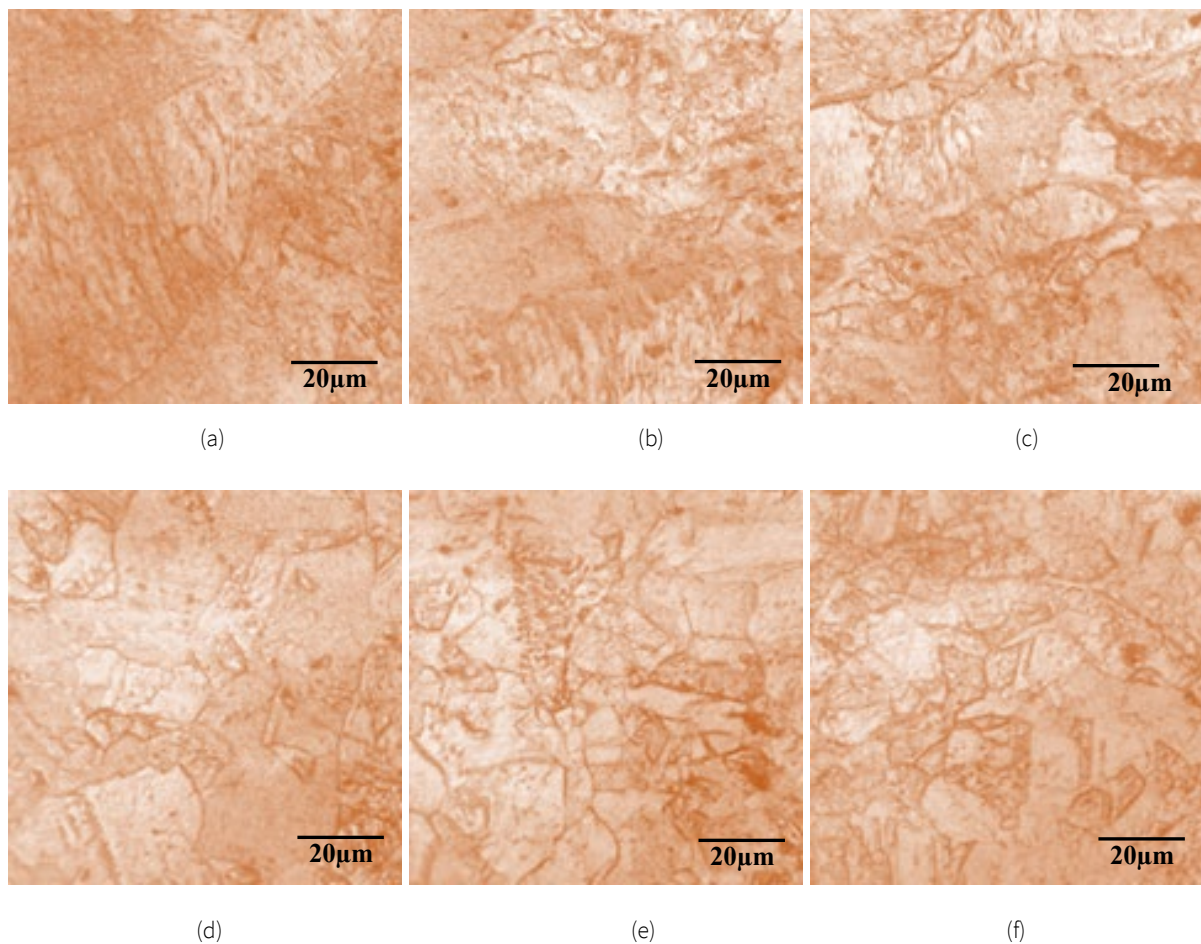
Figure 1. Optical micrograph of 80% cold rolled (a) commercially pure Cu, (b) tin affected Cu-0.26Sn and (c) Cu-0.57Sn alloys, aged at 400°C for one hour (d) commercially pure Cu, (e) tin affected Cu-0.26Sn and (f) Cu-0.57Sn alloys.

(a)

(b)

(c)
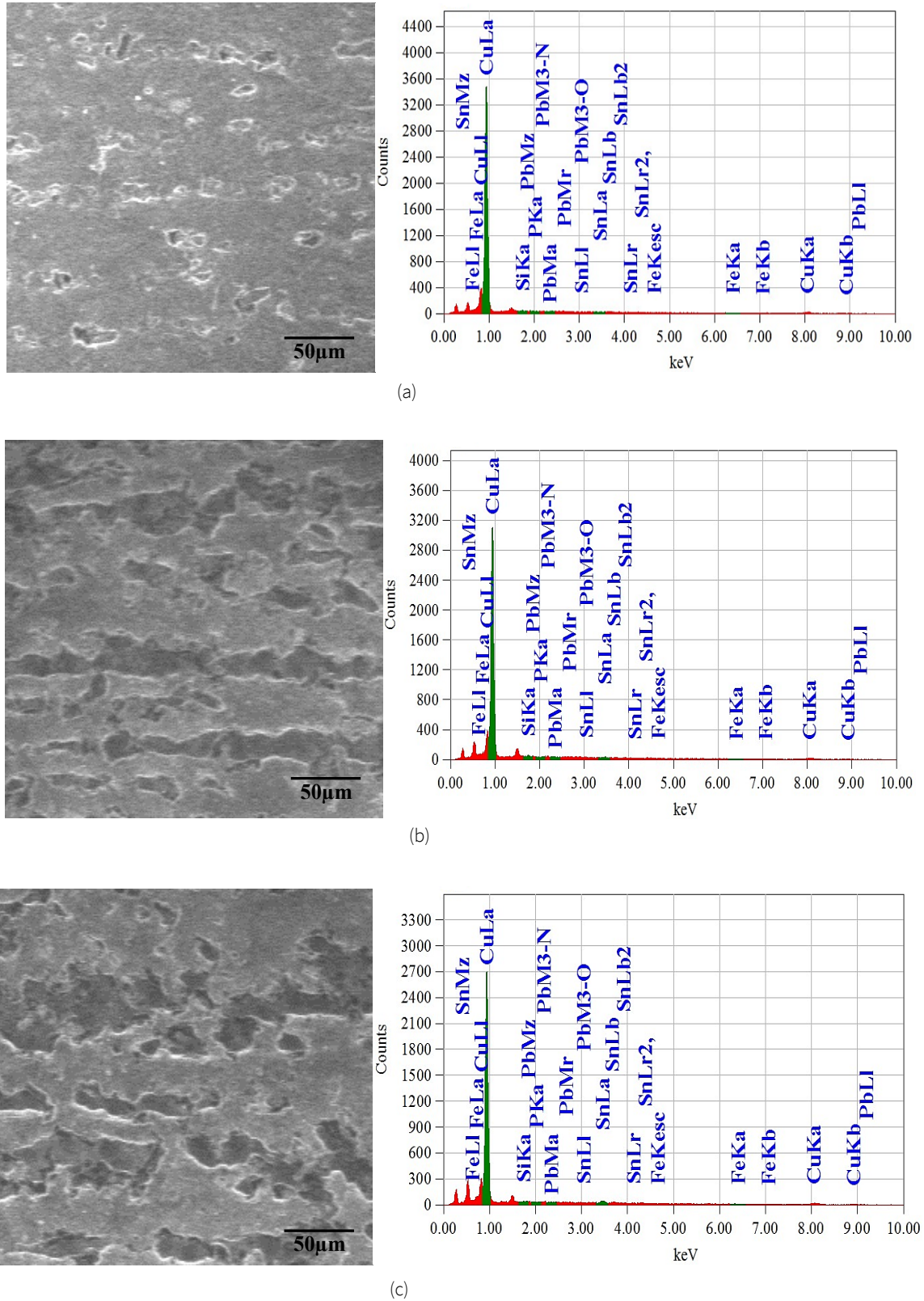
Figure 2. SEM images of the cold rolled and aged at 200°C for one hour (a) commercially pure Cu, (b) tin affected Cu-0.26Sn and (c) Cu-0.57Sn alloys.

3.2. Cold rolling

The variation of micro-hardness and electrical resistivity values with the different cold deformations of Cu and both binary Cu-0.26Sn and Cu-0.57Sn alloys is plotted in Fig. 3. The average hardness of the samples increases with the degree of deformation, where trace addition demonstrates a higher rate (Fig. 3a). It may be clarified first as the cold rolling results in a decrease in grain size, and the grain boundary increases with an increase in rolling reduction. The smaller grain size is more effective at inhibiting dislocation movement and multiplication, resulting in enhanced hardness. Then, the density of dislocations was remarkably increased during cold rolling. Furthermore, the existing dislocations hinder the nucleation and movement of new dislocations, leading to the increased hardness of this material. Additionally, the development of texture orientation due to cold rolling has an effective role in improving the hardness of the alloys. Higher hardness values are obtained with small added alloys than Cu because the elements create additional dislocations. The initial superior hardness of the Sn added alloys occurred due to the solute solution strengthening and the higher size of atoms than Cu in the alloys (Rahman et al., 2021). However, Sn shows superior hardness because of the dissimilar crystal orientation of the BCC of Sn precipitated within the FCC Cu matrix. β-Sn precipitates might have generated coherency strain which leads to higher hardness in this alloy.

The increase in hardness rates is notably prominent when subjecting alloys with higher Sn content to cold rolling processes. This rise in hardness can be primarily ascribed to the synergistic influence exerted on both the alloy matrix and its precipitates. This results in the accumulation of a greater number of dislocations and twins within the material, alongside an increased abundance of smaller and more refined precipitates dispersed throughout the alloy structure (Haque et al., 2022; Leineweber, 2023; Zheng et al., 2020).

The average values of electrical resistivity of the samples decrease initially to some extent, followed by an increase with the degree of deformation (Fig. 3b). Cast alloys normally contain pinhole or porosity like defects due to casting. Cold rolling or plastically deformation decreases the porosity, resulting in better contact between the atoms, which decreases the alloy's electrical resistivity. Under extreme degrees of deformation, the material developed defect through higher dislocation density and sub-grain boundaries. The findings mentioned above were published in 2021 by Karthik et al. (2021) after conducting a transmission electron microscopy study on Cu-Sn alloys, as well as on Cu–Sn–Ti and Cu–Sn–Zn alloys. As a result, the electron scattering into the material increases, resulting in an increase in resistivity. This is due to distortion of the lattice structure or internal damage. Disc values are the result of two opposing effects. The electrical resistance seems to decrease as a result of the first

effect appearing to be stronger than the second. It also shows that the electrical resistance of Cu is lower than that of alloys with trace addition because the presence of other elements in the alloy always reduces electrical conductivity. Solid solution strengthening distorts the lattice and provides resistance to dislocation motion. As is typically observed, an increased level of Sn serves to boost the resistivity properties, especially when coupled with the added impact of a more pronounced fluctuating nature resulting from the process of cold rolling. The reduction in rolling increases means plastically deformed materials are more deformed, resulting in an increased dislocation density inside a material, making it more destroyed (Haque et al., 2022; Nestorović, 2004). It is worth mentioning that when considering commercially pure aluminum, the behavior of dislocation density within the material becomes increasingly disrupted as observed through numerical analysis performed by Sidor et al. (2021).

(a)

(b)
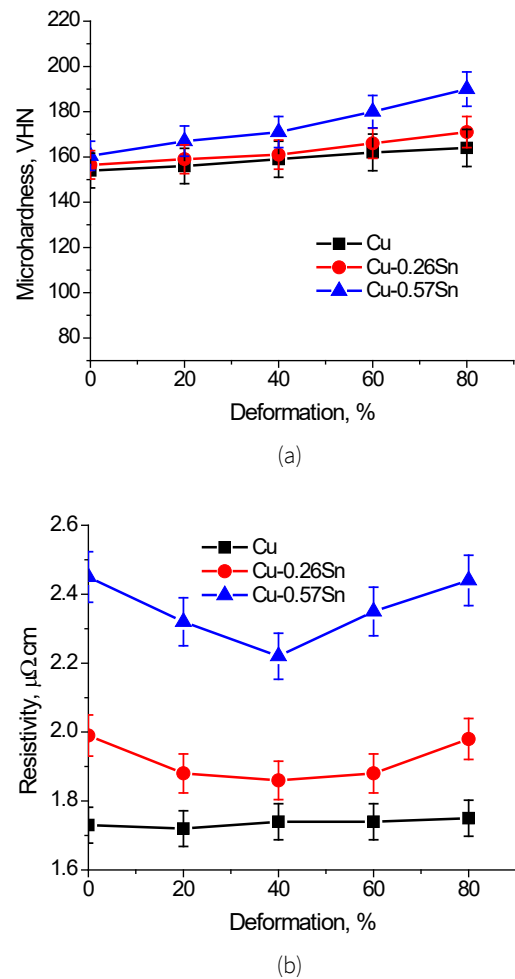
Figure 3. Fluctuations of (a) Micro-hardness and (b) Electrical resistivity of commercially pure Cu, tin added Cu-0.26Sn and Cu-0.57Sn alloys under cold rolling.

3.3. Thermal ageing
3.3.1. Isochronal ageing

The microhardness and resistivity values of 80% cold-rolled samples at isochronally ageing treatment for a period of one hour are presented in Fig 4. Evidently, all samples show a small softening during the initial stage of ageing, then increase in hardness after ageing at 150°C. Commercially pure Cu attains an almost negligible increase in hardness rather than a drastic fall when the ageing temperature increases. But alloys containing Sn hold the strength up to 250°C followed by a profound decrease in hardness (Fig. 4a). Similarly, the initial softening of the alloys during isochronal ageing is thought to be due to dislocations rearrangement and GP zone dissolution at the ageing temperature (Kaiser & Kaiser, 2021). During casting alloys are accumulated some impurities from the environment like Al, Pb, P, Si, Zn etc. Cu forms different hint intermetallics as well as GP zones, which increase the hardness of pure Cu. In case of Sn doped Cu samples, the ageing phenomenon can be clarified via the dislocation theory. Through solidification and ageing treatment, Sn forms solid solution phases α-Cu and β-Sn the complex crystal structures, and the stable main intermediate phases Cu_3Sn, $Cu_{41}Sn_{11}$, $Cu_{10}Sn_3$, and Cu_6Sn_5 (Leineweber, 2023). But two intermetallics, Cu_3Sn and Cu_6Sn_5 in particular, play the most important role in increasing hardness. The level of these intermetallics depends on the amount of Sn addition in the alloys. Additionally, Sn forms intermetallics during ageing with trace impurities by way of the casting environment. These fine intermetallic precipitates act as a barrier to dislocation movement, preventing the softening of the samples. Plastically deformed alloys usually have huge dislocations and more subgrain formation as affected by the grain orientation, which has an important role in the resulting high hardness. High temperature aging can be associated with stress relief, dislocation rearrangement, recovery, and grain growth in alloys. As recovery progresses, the deformed grains soften, and the subgrains rotate and change to a new orientation. Recrystallization becomes more complete with aging at 350 °C (Ahmed et al., 2021; Yang et al., 2023).

The results of the electrical resistivity of the samples allied to isochronal ageing are presented in Fig. 4b. The copper sample shows a continuous reduction in resistivity. The initial rate of reduction is low for dislocations rearrangements within cold worked alloys, and later the rate of reduction increases due to recovery and recrystallization. Tin added alloys demonstrate the initial reduction of resistivity due to dislocation rearrangement, the next increase due to intermetallic formation, followed by the reduction associated with precipitation coarsening, recovery, and recrystallization. According to classical electronic theory, it may be stated that conductivity is proportional to the density of free electrons and the average free route into the material,

whereas resistivity depends on the collision of electrons with the lattice (Palenskis, 2022). These intermetallics also cause the lattice's electric field to be non-uniform and intensify the scattering of electron waves, which raises the material's resistivity. Recovery reduces the concentration of the grain defect and the unevenness of the lattice. Additionally, recrystallization can remove crystal grains and lattice deformation, eventually restoring the microstructure to its pre-cold rolling condition and as a result, decreasing electrical resistance (Kaiser, 2020). In the case of the alloys to which 0.57Sn has been added, a more pronounced rate of increase and decrease is frequently noticed. This phenomenon can be attributed to the enhanced efficiency of the precipitates in addition to the improvement in recovery mechanisms.
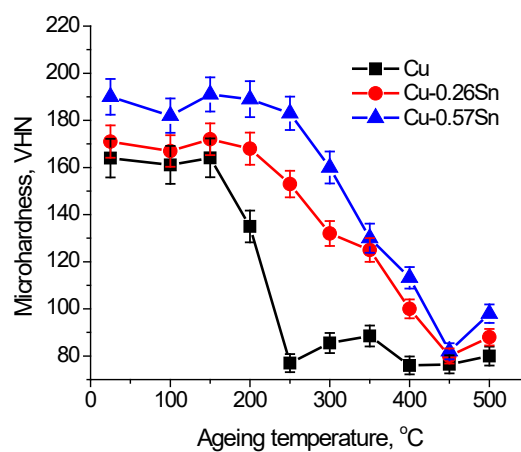
(a)
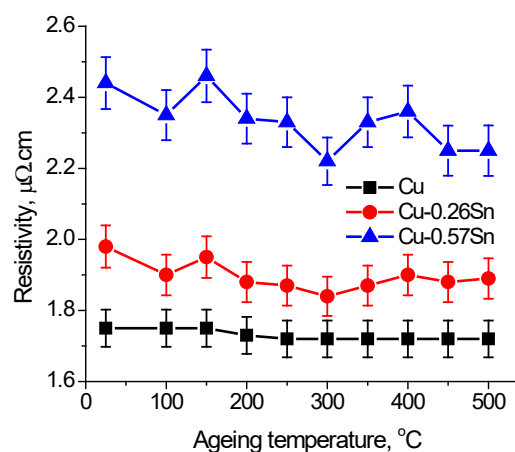
(b)

Figure 4. Fluctuations of (a) hardness and (b) resistivity of experimental Cu and other two Cu-alloys due to the isochronally ageing of alloys for 1 hour.

3.3.2. Isothermal ageing

In isothermal ageing at 150°C and 200°C, the effect of time-span on the microhardness of the cold rolled alloys is displayed in Fig. 3. The results of both isochronal and isothermal ageing of alloys are fully related to the isothermal ageing response. All alloys exhibit an initial softening to dissolve the GP zone and relieve stress, followed by an increase in microhardness properties through the formation of intermetallic compounds. During the long aging process, softening occurs due to the recovery process of the alloy. At the lower ageing temperature of 150°C, all these events occur later (Fig. 5a). The increase in hardness ageing after 240 min is noted in the Sn treated alloys. Aged at 200°C hardness peaks are noted once again in short time, like 30 minutes (Fig. 5b). At higher aging temperatures, the dissolution of the GP zone, the formation of various metastable phases, and the recovery occur faster. This makes perfect sense given that as the temperature rises, the molecules gain energy and accelerate. Therefore, the likelihood of molecules moving with the activation energy needed to trigger the reaction during collisions increases as temperature rises. (Ahmed et al., 2021; Rahman et al., 2021). It is important to reveal that pure Cu starts to soften significantly after 30 minutes at an aging temperature of 200°C for recovery and recrystallization. The Sn doped alloys continue to withstand ageing and softening caused by the different fine Cu_xSn_y intermetallic precipitates that form during solidification and ageing. These precipitates prevent dislocation slip, maintain stable intermediate sub boundaries, and provide resistance to recovery, grain growth, and recrystallization of the alloys (Kaiser & Rashed, 2022).

Again, the phenomena of electrical resistivity under both the isothermal aging treatment at 150 °C and 200 °C of three samples are presented in Fig. 6. It fully complies with the nature of hardness variation under those ageing treatments. At the initial stage, the drop in resistivity for all the samples is related to stress reliving along with recovery. Except for the base sample of Cu, both alloys with added Sn show some increase in resistivity by reason of precipitate formation. This decrease in resistivity for all the samples is due to precipitate coarsening. Obviously, the higher percentage of added Sn displays the higher intensity of both drop and the increase in resistivity for its higher occurrence. After some time, resistivity goes to a constant character as not enough is affected by this temperature. It should be mentioned that ageing at a higher temperature 200°C, all happens earlier than ageing at lower temperature 150°C. Higher ageing temperatures accelerate dislocation rearrangement as well as precipitation formation; as a result, these occur earlier. Similar findings associated with the Cu alloys were also reported earlier by Rahman et al. (2021) and other non-ferrous materials by Kaiser and Rashed (2022).

3.4. Reflectance behavior

The reflectance power of pure Cu and the other two Sn added alloy samples was measured with the wavelength. Figure 7a displays those changes ranging from the infrared region to the 220-800 nm wavelength. The graph clearly displays that the reflectance of the samples increased gradually with the wavelength. As the wavelength increases, the refractive index becomes smaller, which leads to an increase in reflectance (Wu et al., 2010).

(a)   (b)
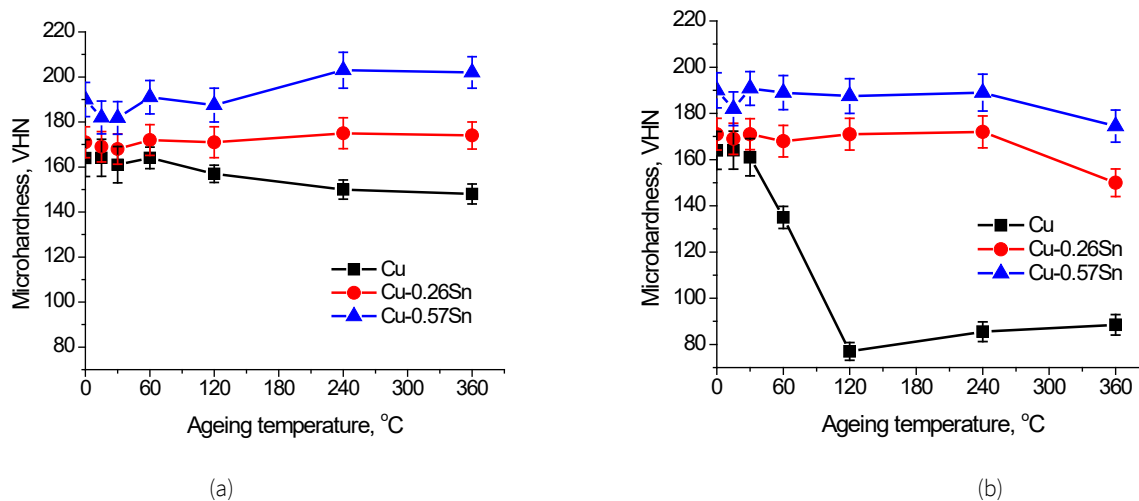
Figure 5. Hardness fluctuations of experimental Cu and other two Cu-alloys due to isothermal aging at (a) 150 °C and (b) 200 °C.
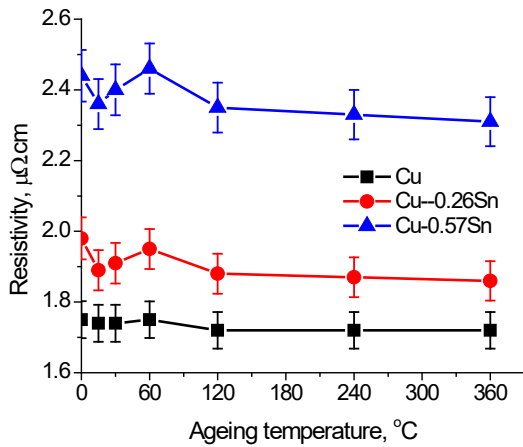
(a)
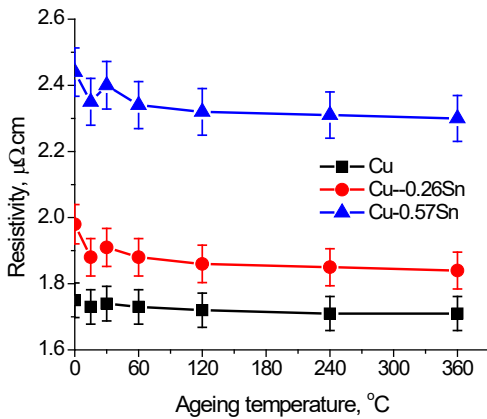
(b)

Figure 6. Resistivity fluctuations of experimental Cu and other two Cu-alloys due to isothermal aging at (a) 150 °C and (b) 200 °C.

At any given wavelength, the profiles of the total reflectance curves for three samples are similar in nature, copper shows the highest intensity of reflectance, whereas the Sn added alloys show the lowest as well as the highest when the amount of Sn is increased. Once pure Cu is affected by Sn, the reflectance property goes downward. It is generally known, light that is incident on a surface and reflected at an interface is referred to as reflectance. The sample absorbs, scatters, or transmits any light that is not reflected. High specular reflectance, or the ability of incident light to reflect in the same direction, is found on very smooth surfaces. When light strikes a rough or matte surface, diffuse reflection takes place, dispersing the light in all directions. Most surfaces exhibit both diffuse and specular reflections. The addition of Sn changed the sample's structural homogeneity and deteriorate the crystallinity of Cu, which led to a decrease in reflectance (Choi et al., 2019).

Again, Fig. 7b represents changes in reflectance with the ageing temperature of the samples. The primary color of Cu, which has a wavelength between 620 and 750 nm, is extremely close to red. The wavelength of 700 nm is chosen as the average value to represent this color region. The mean spectral reflectance was considered in the red region at a constant wavelength of 700nm. As the annealing temperature increases, it is observed that the reflectance first increases, then decreases in nature, and finally increases, followed by a constant value. The evidence supports the idea that the initial ageing causes the stress reliving that makes the material rather defect free; additionally, fine precipitates are stated to form uniformly distributed within the alloys. Both are favorable increasing the reflectance behavior of the materials. As the aging temperature increases, the precipitates begin to coarsen and allow them to concentrate together, resulting in the formation of fine precipitate-free areas in the alloy matrix. This inhomogeneity of the alloy surface reduces the reflectivity (Cooper & Mustard, 1999). Finally, increased and constant values of reflectance, subjected to high aging temperatures, make the grains completely recrystallized, meaning that most regions are free of defects and reach the ideal crystalline state (Choi et al., 2019).
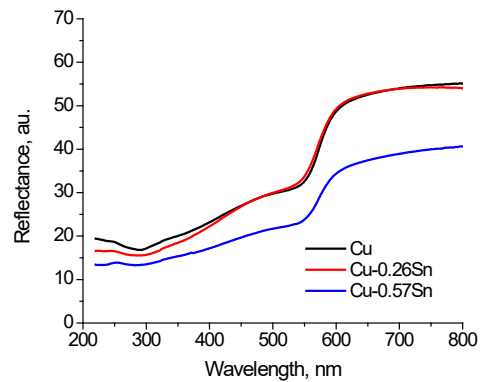
(a)
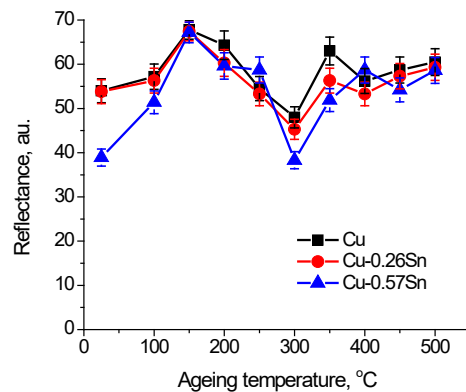
(b)

Figure 7. Reflectance behavior of the samples as a function of (a) wavelength and (b) ageing temperature at 700nm wavelength.

3.5. DSC study

Figure 8 shows the DSC heating scan curve of Cu and the other two Sn added cold rolled alloys without any ageing treatment. All samples achieve an endothermic peak around 60°C, which is attributed to GP zone dissolution (Zhu et al., 2018). It has already been discussed that all the samples consist of different trace impurities that help form the GP zones. The activation energies for the dissolution process of Cu, Cu-0.26Sn and Cu-0.57Sn alloys are 59.5, 63.1, and 66.1 kJ/mol respectively, as they are closed to the activation energies for dissolution of GP zone, 64.3 kJ/mol as reported earlier (Ma et al., 2021). Again, all alloys attain an exothermal peak due to precipitate formation around 120°C. The activation energy of this process as metastable phase formation, as reported in a previous study, was 34.8 kJ/mol (Espiritu & Amorsolo, 2019). The activation energy of this course is close to 36.5, 41.1, 43.3 kJ/mol respectively. Both Tin-added alloys show an endothermic peak around 230°C, with the activation energy of this process being around 78.3 kJ/mol (Tan et al., 2015). More especially, it can be conveyed that the melting temperature of Sn is 232°C.

Finally, commercially pure Cu, Cu-0.26Sn and Cu-0.7Sn alloys attain the exothermic peak around 420°C, 500°C and 510°C with activation energies of 98 KJ/mol, 117 KJ/mol and 120 KJ/mol, respectively, for the recrystallization process. For the cold rolled highly pure Cu the activation energy of 90 KJ/mol is for recrystallisation reported earlier (Krishna et al., 2024). Although 400°C is said to be the ideal temperature for recrystallization, it actually occurs at a high temperature of 450°C. It is also observed that the activation energy for recrystallization in this specific instance is likewise fairly high. As a result, in Sn affected alloys, recrystallization kinetics are significantly delayed. This is so because fine, coherent precipitates have high coherency strains. This severely impedes the migration of dislocations. The dissolution of GP zones and the formation of metastable phases in Sn-doped alloys also display the tendency to occur at higher temperatures and activation energies. Since the alloying element has a larger size than copper, distortions in the matrix result, which act as obstructions to dislocation movement and thereby delay diffusion. So, higher energy is needed to increase the resulting activation energy to a higher level.

3.6. XRD study

Ageing at 200°C for one hour of the 80% cold-rolled Cu and both the Sn-added alloys is characterized by an X-ray diffractometer. The obtained XRD patterns within a 20-to-85-degree angle at room temperature are demonstrated in Fig. 9. It can be seen from the figure commercially, Cu contains three peaks, as reported earlier, around 43.3°, 50.5°, and 74.1°, which correspond to the (111), (200), and (220) planes, respectively, which can be indexed to the FCC structure of Cu (Dong et al., 2018). But the tin-added alloy shows the additional peaks of Sn and its intermetallics in the XRD pattern. It is noted that except for Cu, the intensity of these elements is very low for the little amount they present in the Cu-alloys. Additionally, there is no remarkable sign of any intermetallics in the XRD pattern, as the trace amounts are relatively insignificant, and cannot be seen with the naked eye. This finding was also reported by earlier investigators (Lei et al., 2014). One thing that may be noted is that due to the addition of Sn, the intensity of the first peak of Cu reduces and the intensity of Sn phases increases.
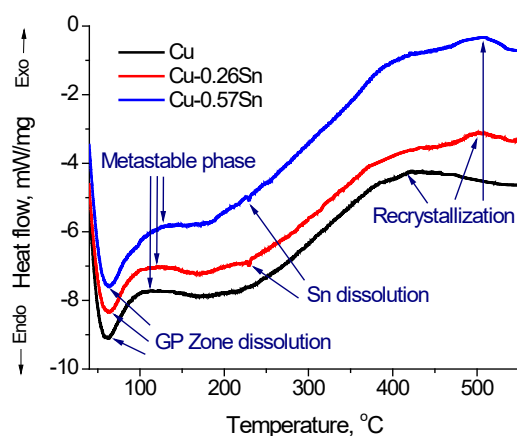
Figure 8. DSC heating curve of experimental Cu and other two Cu-alloys.
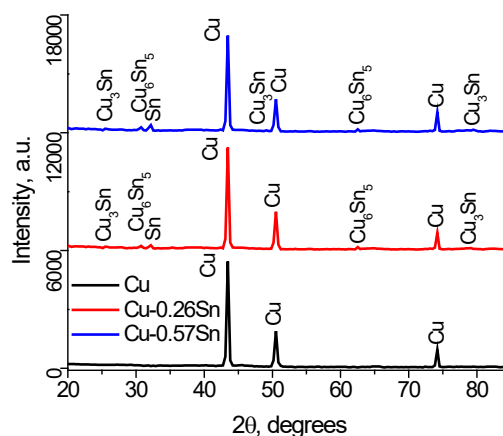
Figure 9. The XRD patterns of the experimental Cu and other two Cu-alloys.

4. Conclusions

The effect of tin-based lead-free solder on the physical properties of Cu was surveyed, and the main results are:

Sn has a positive effect on the hardness of pure Cu owing to solid solution strengthening. Cold rolling of higher Sn added alloys form the complex structure as a result, the rate of hardness and electrical resistivity are higher.

During solidification and ageing Sn forms different intermetallics, specially the two most important intermetallics, Cu_3Sn and Cu_6Sn_5 dominate the higher hardness. Maximum hardness is achieved when the Sn-doped alloys are isothermally aged at least at 150 °C for 240 min or at 200 °C for 30 min. Similarly, the resistivity also shows the highest at those states.

The fine precipitates act as a barrier to dislocation movement, and as a result, increase the recrystallization temperature, preventing the softening of the Sn-doped samples. Because of the development of fine precipitates, electrical resistivity increased, but at higher ageing temperature, it decreased due to precipitate coarsening as well as recovery and recrystalization.

The reflectance property of Cu goes downward when affected by Sn, changing the structural homogeneity and deteriorating crystallinity of Cu, but ageing at a higher temperature reduces the difference in these properties because it reaches a defect-free and ideal crystalline state.

Equiaxed grains are elongated in the rolling direction due to plastic deformation, which causes the crystal grains to blur, making them difficult to distinguish. All alloys have reached a fully recrystallized state after annealing at 400°C for one hour, but the Sn doped alloys demonstrate a higher fraction of the dissolved second phase in the microstructure and developed grain boundaries.

Conflict of interest

The author has no competing interests to declare relevant to this article's content.

Acknowledgements

Funding

References

Ahmed, A., Iqbal N., Kaiser M. S., & Ahmed S. R., (2021). Thermo-mechanical and optical characteristics of cold-rolled copper with natural melting impurities, *AIP Conference Proceedings*, 2324 (1), 0300171-7.
https://doi.org/10.1063/5.0037516

Cañadilla, A., Romero, A., Rodríguez, G. P., Caminero, M. Á., & Dura, Ó. J. (2022). Mechanical, electrical, and thermal characterization of pure copper parts manufactured via material extrusion additive manufacturing. *Materials, 15*(13), 4644.
https://doi.org/10.3390/ma15134644

Choi, G. M., Kim, D. G., Im, B., & Chae, H. J. (2019). Reflectance characteristics of al alloys containing Si, Mg, Cu, and lanthanide (Nd, Sm, Gd) for 3D printing. *Metals and Materials International*, *25*, 946-955.
https://doi.org/10.1007/s12540-019-00256-9

Cooper, C. D. & Mustard, J. F. (1999). Effects of Very Fine Particle Size on Reflectance Spectra of Smectite and Palagonitic Soil, *Icarus*, *142*(2), 557-570.
https://doi.org/10.1006/icar.1999.6221

Davis, J. R. (1998). Introduction and Overview of Copper and Copper Alloys. *Metals Handbook, Desk Edition, ASM International, Materials Park, Ohio, USA.*
https://doi.org/10.31399/asm.hb.mhde2.9781627081993

Dong, Y., Wang, K., Tan, Y., Wang, Q., Li, J., Mark, H. & Zhang, S. (2018). Synthesis and Characterization of Pure Copper Nanostructures Using Wood Inherent Architecture as a Natural Template. Nanoscale Research Letters, 13, 119, 1-8.
https://doi.org/10.1186/s11671-018-2543-0

Espiritu, R. & Amorsolo, A. (2019). Fabrication and characterization of Cu–Zn–Sn shape memory alloys via an electrodeposition–annealing route. *International Journal of Minerals, Metallurgy and Materials*, 26, 1436-1449.
https://doi.org/10.1007/s12613-019-1886-6

Haque, M. S., Khan, S. A. R., & Kaiser, M. S. (2022). Effect of Sc and Zr on precipitation behaviour of wrought Al-bronze. In *IOP Conference Series: Materials Science and Engineering* (Vol. 1248, No. 1, p. 012037). IOP Publishing.
https://doi.org/10.1088/1757-899X/1248/1/012037

Kaiser, M. S. (2020). Trace impurity effect on the precipitation behaviour of commercially pure aluminium through repeated melting. *European Journal of Materials Science and Engineering*, 5(1), 37-48.

Kaiser, S., & Kaiser, M. S. (2021). Impact of cold plastic deformation and thermal post-treatment on the physical properties of copper based alloys Al-bronze and α-brass. *Journal of Acta Metallurgica Slovaca*, 27(3), 114-121. https://doi.org/10.36547/ams.27.3.951

Kaiser, S., & Kaiser, M. S. (2020). Influence of aluminium and zinc additives on the physical and thermal behaviour of cast copper. *Journal of Sustainable Structures and Materials*, *3*(1), 1-9.

Kaiser, M. S. & Rashed, H. M. M. A. (2022). Precipitation Behavior of Prior to Hot Roll in Cold Rolled Al-Mg and Al-Mg-Zr Alloys. *Kovove Materialy - Metallic Materials*, 60(4), 247-256.

Karthik, M., Abhinav, J. & Shankar, K. V., (2021). Morphological and Mechanical Behaviour of Cu-Sn Alloys—A review. Metals and Materials International, 27, 1915-1946. https://doi.org/10.1007/s12540-020-00899-z

Komesu, A., Martinez, P. F. M., Lunelli, B. H., Oliveira, J., Maciel, M. R. W., & Filho, R. M. (2017). Study of Lactic Acid Thermal Behavior Using Thermoanalytical Techniques. *Journal of Chemistry*, 2017(4149592), 1-7. https://doi.org/10.1155/2017/4149592

Krishna, S. C., Yasam, P., Dudala, S., Kotla S., Muneshwar P., Pant B., & Korla, R., (2024). Recrystallization Behavior of Cold-Rolled Cu-Cr-Nb-Zr Alloy Investigated by Differential Scanning Calorimetry, *Journal of Materials Engineering and Performance*, *33*, 136–143. https://doi.org/10.1007/s11665-023-07981-8

Lei, W. X., Pan, Y., Zhou Y. C., Zhou, W., Peng, M. L. & Ma, Z. S. (2014). CNTs–Cu composite layer enhanced Sn–Cu alloy as high performance anode materials for lithium-ion batteries, RSC Advances, 4(7), 3233-3237. https://doi.org/10.1039/C3RA44431G

Leineweber A., (2023). The Cu–Sn System: A Comprehensive Review of the Crystal Structures of its Stable and Metastable Phases. *Journal of Phase Equilibria and Diffusion*, 44, 343-393. https://doi.org/10.1007/s11669-023-01041-3

Ma, Y., Huang, Y., & Zhang, X. (2021). Precipitation thermodynamics and kinetics of the second phase of Al–Zn–Mg–Cu–Sc–Zr–Ti aluminum alloy. *Journal of Materials Research and Technology*, 10, 445-452. https://doi.org/10.1016/j.jmrt.2020.11.075

Nai, S. M. L., Tan, L. B. & Selvanayagam, C. (2015). Solder Joint Technology. In: Nee, A. (eds) Handbook of Manufacturing Engineering and Technology. *Springer*, London. https://doi.org/10.1007/978-1-4471-4670-4_59

Narayan, S & Prabhu, K. N. (2013). Comparison of spreading behaviour and development of interfacial microstructure in Sn-0.7 Cu, Sn-0.3 Ag-0.7 Cu and Sn-2.5 Ag-0.5 Cu lead-free solder alloys on Fe-42Ni substrate. *Materials Science and Technology*, *29*(4), 464-473. https://doi.org/10.1179/1743284712Y.0000000162

Nestorović, S. (2004). Influence of deformation degree at cold-rolling on the anneal hardening effect in sintered copper-based alloys. *Journal of Mining and Metallurgy, Section B: Metallurgy*, *40*(1), 101-109.

Palenskis, V. (2022). Free Electron Characteristic Peculiarities Caused by Lattice Vibrations in Metals. *World Journal of Condensed Matter Physics*, 12(02), 9-17. https://doi.org/10.4236/wjcmp.2022.122002

Peng, J., Li, J., Liu, B., Fang, Q., & Liaw, P. K., (2024). Origin of thermal deformation induced crystallization and microstructure formation in additive manufactured FCC, BCC, HCP metals and its alloys. *International Journal of Plasticity*, 172, 1-21. https://doi.org/10.1016/j.ijplas.2023.103831

Rahman, M. M., Ahmed, S. R., & Kaiser, M. S. (2021). On the Investigation of Reuse Potential of SnPb-Solder Affected Copper Subjected to Work-Hardening and Thermal Ageing. *Materials Characterization*, 172, 2021. https://doi.org/10.1016/j.matchar.2021.110878

Sakib-Uz-Zaman, C., & Khondoker, M. A. H. (2023). A review on extrusion additive manufacturing of pure copper. *Metals*, *13*(5), 859. https://doi.org/10.3390/met13050859

Satyanarayan & Prabhu, K. N. (2013). Study of Reactive Wetting of Sn-0.7 Cu and Sn-0.3 Ag-0.7 Cu Lead Free Solders during Solidification on Nickel Coated Al Substrates. In *Proceedings of World Academy of Science, Engineering and Technology* (No. 73, p. 952). World Academy of Science, Engineering and Technology (WASET). 7, (1), 25-28.

Satyanarayan & Prabhu, K.N. (2012a). Effect of temperature and substrate surface texture on wettability and morphology of IMCs between Sn–0.7Cu solder alloy and copper substrate. *Journal of Materials Science: Materials in Electronics*, 23, 1664-1672. https://doi.org/10.1007/s10854-012-0644-6

Satyanarayan, & Prabhu, K. N. (2012b). Wetting Characteristics of Sn-0.7Cu Lead-Free Solder Alloy on Copper Substrates, *Materials Science Forum*, 710, 569–574. https://doi.org/10.4028/www.scientific.net/MSF.710.569

Satyanarayan & Prabhu, K. N., (2011). Reactive wetting, evolution of interfacial and bulk IMCs and their effect on mechanical properties of eutectic Sn-Cu solder alloy. Advances in Colloid and Interface Science, 166(1-2), 87-118. https://doi.org/10.1016/j.cis.2011.05.005

Sidor, J. J., Chakravarty, P., Bátorfi, J. G., Nagy, P., Xie, Q. & Gubicza, J. (2021). Assessment of Dislocation Density by Various Techniques in Cold Rolled 1050 Aluminum Alloy. *Metals, 11(*1571), 1-16. https://doi.org/10.3390/met11101571

Tan, A. T., Tan, A. W. & Yusof, F. (2015) Influence of nanoparticle addition on the formation and growth of intermetallic compounds (IMCs) in Cu/Sn–Ag–Cu/Cu solder joint during different thermal conditions*, Science and Technology of Advanced Materials*, 16(3). https://doi.org/10.1088/1468-6996/16/3/033505

Tehrani, M. (2020). Advanced electrical conductors. An overview and prospects of metal nanocomposite and nanocarbon based conductors. Physica Status Solidi. A, Applications and Materials, 218(8), 1-17. https://doi.org/10.1002/pssa.202000704

Wu, C. Y., Jacobson, A. R., Laba, M., Kim, B. & Baveye, P. C., (2010). Surrogate Correlations and Near-Infrared Diffuse Reflectance Sensing of Trace Metal Content in Soils. Water Air and Soil Pollution, 209, 377-390. https://doi.org/10.1007/s11270-009-0206-6

Yang, P., He, D., Shao, W., Tan, Z., Guo, X., Lu, S., & Anton, K., (2023). Study of the microstructure and mechanical properties of Cu–Sn alloys formed by selective laser melting with different Sn contents. *Journal of Materials Research and Technology*, 24, 5476-5485. https://doi.org/10.1016/j.jmrt.2023.04.198

Zhang, H., Chen, L., Liu Y. & Li, Y. (2013). Experimental study on heat transfer performance of lotus-type porous copper heat sink, International Journal of Heat and Mass Transfer, 56(1-2), 172-180, https://doi.org/10.1016/j.ijheatmasstransfer.2012.08.047

Zhao, M., Zhang, L., Liu, Z. Q., Xiong, M. Y., & Sun, L. (2019). Structure and properties of Sn-Cu lead-free solders in electronics packaging. *Science and technology of advanced materials*, *20*(1), 421-444. https://doi.org/10.1080/14686996.2019.1591168

Zheng, Z., Guo, P., Li, J., Yang, T., Song, Z., Xu, C., & Zhou, M. (2020). Effect of cold rolling on microstructure and mechanical properties of a Cu–Zn–Sn–Ni–Co–Si alloy for interconnecting devices. *Journal of Alloys and Compounds*, *831*, 154842. https://doi.org/10.1016/j.jallcom.2020.154842

Zhu, Z., Cai, Y., Sui, Y., Song, K., Zhou, Y. & Zou, J. (2018). Precipitation Characteristics of the Metastable γ" Phase in a Cu-Ni-Be Alloy, *Materials*, 11(1394), 1-14. https://doi.org/10.3390/ma11081394

Zhu, Z., Cai, Y., Sui, Y., Song, K., Zhou, Y., & Zou, J. (2018). Precipitation Characteristics of the Metastable γ "Phase in a Cu-Ni-Be Alloy. *Materials*, *11*(8), 1394. https://doi.org/10.3390/ma11081394